Morphological instability of growth fronts due to stress-induced mobility variations

Jennifer F. Sage, William Barvosa-Carter,[a] and Michael J. Aziz[b]
Division of Engineering and Applied Sciences, Harvard University, Cambridge, Massachusetts 02138

(Received 20 March 2000; accepted for publication 30 May 2000)

We report a comparison between theory and experiment for a general stress-induced morphological growth instability that is kinetically rather than energetically driven. Stress variations along a perturbed planar growth front result in variations in interfacial mobility in a manner that is destabilizing under one sign of the stress state and stabilizing under the opposite sign, even for a pure material. Investigation of solid-phase epitaxial growth at a corrugated Si(001) interface under both compression and tension results in good agreement between experiment and theory with no adjustable parameters, demonstrating that this mobility-based mechanism is dominant in determining morphological evolution in this system. © *2000 American Institute of Physics.* [S0003-6951(00)01930-6]

There is increasing interest in the effects of nonhydrostatic stresses on condensed phase processes such as diffusion and crystal growth. The focus of most work has been to understand and account for stress effects on the energetics, or driving forces, for these processes, one effect of which is to produce an elastic strain energy driven morphological instability on the surface of strained solids.[1] We have previously called attention to the mobilities of the interfaces or atoms involved in growth[2,3] and characterized the stress dependence of mobilities,[3–7] and we and others have predicted how the changes in mobility due to stress also help determine the growth morphology of a solid.[5,8–14] Here, we report results of growth under biaxial tension that confirm that the morphological stability or instability for solid-phase epitaxial growth (SPEG) of Si(001) is dominated by the stress dependence of the mobility and not by the energetics of elastic strain energy minimization. We avoid the potential complications associated with the coupling of strain and composition by studying a single-component system in which stress is applied externally.

Within transition state theory, the dependence upon stress σ of an atomic or interfacial mobility M is characterized by the *activation strain tensor*[3] $V_{ij}^{*} \equiv kT\partial \ln M/\partial\sigma_{ij}$. A positive (negative) V_{11}^{*}, for example, implies that M is reduced (enhanced) upon the application of a compressive σ_{11}. Just such a dependence of the interfacial mobility on stress has been observed[3,5] in SPEG of Si(001), characterized by $V_{11}^{*}=+0.14$ times the atomic volume Ω of crystalline Si.

A positive V_{11}^{*} gives rise to a kinetically driven morphological instability during growth under compressive (i.e., negative) σ_{11}. For a sinusoidally perturbed interface between a growing crystalline phase and a fluid or amorphous parent phase in which stress is at least partially relaxed, or between two elastic phases in which the growing phase has higher moduli, there is a stress concentration in the trough and a stress relaxation at the apex of the perturbation. The stress concentration in the trough results in a local interfacial mobility that is less than that at the apex; hence, the apex grows faster and the perturbation tends to amplify.

The stress effect on mobility is first order in stress, thus giving rise to opposite amplification behavior under tension and compression. In contrast, the energetically driven instability is second order in stress, and therefore, is destabilizing in any stress state. Hence, if the interface is unstable under compression, which is generally observed in many growth situations and specifically known for SPEG,[5,8] and the stress dependence of the mobility is the predominant factor in determining interface instability, then the interface should be stable in tension. This qualitative difference between the kinetically driven and energetically driven instabilities should be observable experimentally.

While spontaneous roughening under stress of an initially planar Si(001) amorphous-crystal (a-c) interface, which never roughens in the absence of stress, is observable, the results are difficult to quantify under the range of readily accessible experimental conditions. Instead, we applied stress to a ''pre-rippled interface'' fabricated by ion implantation of a Si wafer with a lithographically corrugated free surface. By controlling the amplitude and wavelength of the starting interface corrugation, we can make a controlled comparison between theory and experiment for the interface evolution under stress.

Several Si(001) wafers 1 mm thick were patterned using x-ray lithography to create free surfaces corrugated with a series of parallel lines with a repeat distance of $\lambda = 400$ nm. The surface of each wafer was then amorphized by ion implantation (Si^{+}, 90 keV, $2\times10^{15}/cm^{2}$, 77 K) to form a continuous layer of amorphous Si (a-Si). Because of straggling of the incident ions, the initial 25 nm surface corrugation amplitude resulted in a 22 nm corrugation amplitude for the a-c interface, in approximate agreement with the lateral straggle of the ions predicted by simulations.[15] Some of the samples were then diced to form bars 6 mm long with a 1 mm^{2} cross section with the a-Si film occupying one of the long faces and the ripples parallel to the short edge.

A series of these samples was annealed at 520 °C while

[a]Current address: HRL Laboratories, 3011 Malibu Canyon Road, Malibu, CA 90265.
[b]Electronic mail: maziz@harvard.edu

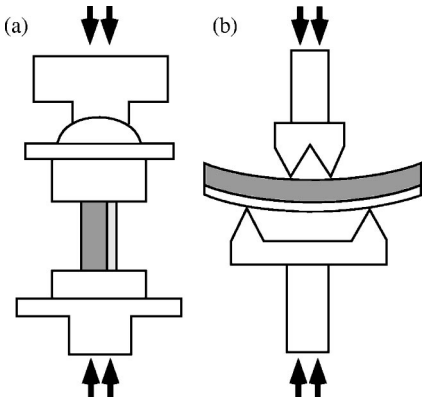

FIG. 1. Apparatus for external application of stress to growth front. (a) Growth under compression. Sample, with amorphous film along right-facing surface, experiences uniaxial compression in the plane of the *a*-*c* interface. The [001] wafer and interface normals point to the right and the wave vector of the ripple is vertical, in either the [100] or [110] direction. (b) Growth under tension. The amorphous-crystal interface is subjected to biaxial tension by loading between two rings. The [001] wafer and interface normals point downward and the [100] wave vector of the ripple points horizontally.

compressed lengthwise, as shown in Fig. 1(a), resulting in a uniaxial stress of -0.5 GPa in the plane of the interface along the wave vector of the corrugation. A control series was annealed under zero stress. A single square sample 22.2 mm on a side and 0.81 mm thick was annealed while being loaded between two rings (diameters 0.25 and 0.125 in.), as shown in Fig. 1(b) with the amorphous side under tension. This configuration resulted in a uniform biaxial[16] stress of $+0.5$ GPa in the plane of the interface in the region within the smaller ring.[17,18] Steel foil (45 μm thick) was placed between the rings and the sample to reduce the stress concentration under the rings, and the sample was protected from reacting with the steel foil by a thin layer of graphite paint. All samples were analyzed using cross-sectional transmission electron microscopy (X-TEM) to measure the interface amplitude and final depth.

In Fig. 2, we show the X-TEM of the initial corrugated interface and the interface after growth in the presence of tensile and compressive stress. The amplitude increases after

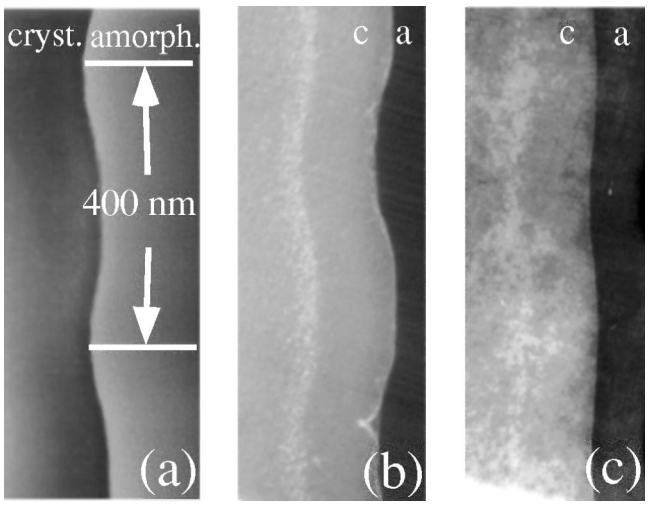

FIG. 2. Cross sections of (a) initial interface, (b) interface after growth under compressive stress ($\sigma_{11} = -0.5$ GPa) showing amplification of perturbation, and (c) interface after growth under tensile stress ($\sigma_{11} = +0.5$ GPa) showing damping of perturbation.

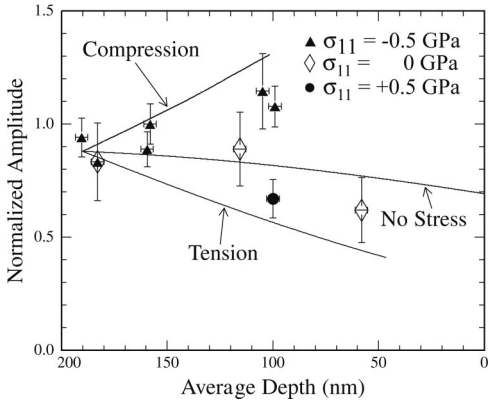

FIG. 3. Perturbation amplitude vs distance regrown. Symbols represent experimental data points, and solid lines are the output of the simulation, which incorporated the maximum possible stress effect arising from the assumption of a fully relaxed amorphous phase.

annealing under compression and decreases after annealing under tension. In Fig. 3, we compile the results for all samples. The reported amplitude of the interface corrugation is divided by the amplitude of the free surface at that point on the wafer, to normalize for sample-to-sample variations in the latter. The abscissa is the average depth of the interface below the free surface, which decreases with time as the crystal consumes the amorphous phase. The samples annealed under compression show a monotonic increase in interface amplitude with time, whereas the amplitude decreases with time for the samples annealed without stress and it decreases even more rapidly for the sample annealed under tension. These results are in qualitative agreement with the predictions of the kinetically driven instability.

In order to provide a more quantitative comparison with theory, a series of simulations was performed to model the interface behavior during growth.[8] The interface is divided into a series of planar segments, each of which is assigned a normal velocity given by the following function of the conditions at its midpoint:

$$\nu \propto \left[f(\theta) \exp\left(\frac{-G^*}{kT} \right) \right] \left[2 \sinh\left(\frac{-\Delta G_{ac}}{2kT} \right) \right], \tag{1}$$

where $f(\theta)$ is the growth kinetic anisotropy function of misorientation θ from (111), G^* is the Gibbs free energy of activation, and ΔG_{ac} is the change in free energy per atom crystallized. G^* includes the stress dependence of the mobility. ΔG_{ac} includes the effects of capillarity, elastic strain energy, and the pressure-volume work due to the interaction of the hydrostatic component of the stress with the small volume drop upon crystallization. A more complete description of the simulation is reported elsewhere.[8]

The local stress state is determined by a boundary integral method.[19] Given the elastic constants of the solid and a set of tractions and displacements as boundary conditions, the remaining unknown surface displacements and tractions are obtained through solving boundary integral equations. The full stress tensor on the boundary is then computed using the formulation presented by Gray *et al.*[20] Stresses in the amorphous phase are assumed to be fully relaxed.

The results of this simulation for the three different stress states are compared in Fig. 3 with the experimental

data. Significantly, the curves represent theoretical upper limits on the effect of stress on the amplitude, due mainly to the assumption of complete stress relaxation in the amorphous phase. They give the maximum expected amplification in the interface corrugation for the compressive case, and the maximum possible stabilization for the tensile case, with no free parameters. Therefore, the prediction is in good quantitative agreement with the experiment. Work is in progress to account for viscous flow in the amorphous phase, which will permit the quantitative prediction of the actual magnitude of, rather than merely upper limits on, the stress effect.

The kinetically driven instability is not the only possible source of an odd-power stress effect. Other possible origins include surface segregation (in alloys) and a nonzero surface stress, which may be large when originating from steps or facets.[21–23] However, these mechanisms are expected to be significant mainly on free surfaces near equilibrium with major surface reconstructions. Although the interface stress of the *a-c* interface is unknown, the effect of even a large interface stress should be insignificant in SPEG because of the large driving force for growth. This expectation is reinforced by our ability to fit our data without considering additional mechanisms.

In conclusion, at least three sources of morphological instabilities must in general be considered in any system: energetically driven instabilities, kinetically driven instabilities, and diffusion field driven instabilities.[24,25] In SPEG, we find that mobility-induced effects dominate the morphological behavior.

This work was supported by Grant NSF-DMR-98-13803 and by the Harvard MRSEC under Grant NSF-DMR-9809363. The authors are grateful to Wen-An Chiou for preparation of a specimen for cross-sectional TEM using the Focused Ion Beam Facility at Northwestern University.

[1] R. J. Asaro and W. A. Tiller, Metall. Trans. A **3**, 1789 (1972).
[2] M. J. Aziz, Appl. Phys. Lett. **70**, 2810 (1997).
[3] M. J. Aziz, P. C. Sabin, and G.-Q. Lu, Phys. Rev. B **44**, 9812 (1991).
[4] M. J. Aziz, S. Circone, and C. B. Agee, Nature (London) **390**, 596 (1997).
[5] W. Barvosa-Carter and M. J. Aziz, Mater. Res. Soc. Symp. Proc. **441**, 75 (1997).
[6] N. Bernstein, M. J. Aziz, and E. Kaxiras, Phys. Rev. B **58**, 4579 (1998).
[7] W. B. Carter and M. J. Aziz, Mater. Res. Soc. Symp. Proc. **356**, 87 (1995).
[8] W. Barvosa-Carter, M. J. Aziz, L. J. Gray, and T. Kaplan, Phys. Rev. Lett. **81**, 1445 (1998).
[9] G. Grinstein, Y. Tu, and J. Tersoff, Phys. Rev. Lett. **81**, 2490 (1998).
[10] V. P. Zhdanov, Phys. Rev. Lett. **83**, 656 (1999).
[11] G. Grinstein, Y. Tu, and J. Tersoff, Phys. Rev. Lett. **83**, 657 (1999).
[12] J. Tersoff, Y. Tu, and G. Grinstein, Appl. Phys. Lett. **73**, 2328 (1998).
[13] H. H. Yu and Z. Suo, J. Appl. Phys. **87**, 1211 (2000).
[14] P. W. Voorhees and M. J. Aziz, in *Conference on Interfaces for the Twenty-First Century*, edited by M. K. Smith and G. B. McFadden (Imperial College, Monterey, CA, 1999).
[15] J. P. Biersack and L. G. Haggmark, Nucl. Instrum. Methods **174**, 257 (1980).
[16] Even though the stress for the sample under tension is biaxial, we can still compare the results to the uniaxial compressive series by decomposing the biaxial stress into components in directions parallel and perpendicular to the corrugation wave vector. The stress component in the direction perpendicular to the wave vector simply increases the overall velocity at all points, but it does not affect the corrugation amplitude because it remains spatially uniform. Only the stress component parallel to the ripple wave vector has different magnitudes at the peaks and troughs and thereby influences the corrugation amplitude.
[17] H. Fessler and D. C. Fricker, J. Am. Ceram. Soc. **67**, 582 (1984).
[18] J. E. Ritter, Jr., K. Jackus, A. Batakis, and N. Bandyopadhyay, J. Non-Cryst. Solids **38&39**, 419 (1980).
[19] J. H. Kane, *Boundary Element Analysis in Engineering Continuum Mechanics* (Prentice-Hall, Englewood Cliffs, NJ, 1998).
[20] L. J. Gray, D. Maroudas, M. N. Enmark, and E. F. D'Azevedo, Eng. Anal. Boundary Elem. **23**, 267 (1999).
[21] Y.-H. Xie, G. H. Gilmer, C. Roland, P. J. Silverman, S. K. Buratto, J. Y. Cheng, E. A. Fitzgerald, A. R. Kortan, S. Schuppler, M. A. Marcus, and P. H. Citrin, Phys. Rev. Lett. **73**, 3006 (1994).
[22] Y.-H. Xie, G. H. Gilmer, C. Roland, P. J. Silverman, S. K. Buratto, J. Y. Cheng, E. A. Fitzgerald, A. R. Kortan, S. Schuppler, M. A. Marcus, and P. H. Citrin, Phys. Rev. Lett. **74**, 4963 (1995).
[23] J. Tersoff, Phys. Rev. Lett. **74**, 4962 (1995).
[24] W. W. Mullins and R. F. Sekerka, J. Appl. Phys. **35**, 444 (1964).
[25] G. S. Bales and A. Zangwill, Phys. Rev. B **41**, 5500 (1990).